Supporting Information

Development of a reactive plume model for the consideration of power-plant plume photochemistry and its applications

Yong H. Kim, Hyun S. Kim, Chul H. Song*

School of Earth Sciences and Environmental Engineering, Gwangju Institute of Science and Technology (GIST), Gwangju 61005, Korea

Shortened title: Development of a reactive plume model

***Corresponding author:** Chul H. Song (chsong@gist.ac.kr)

This document contains 11 pages, 5 tables, and 3 figures.

Estimation of emission rates

In the current study, we have used virtual emissions from the Monticello and Welsh power plants. The calculation of the virtual emission rates was based on flight observations. First, CO_2 emission rates were estimated with an assumption that in-plume CO_2 is not reactive, since the chemical lifetime of CO_2 is much longer than those of other primary pollutants. Also, it was assumed that the plume spreads in a truncated elliptic cone shape and are divided by three sections among the transects (e.g. Transect I and II, Transect II and III, and Transect III and IV), as shown below.

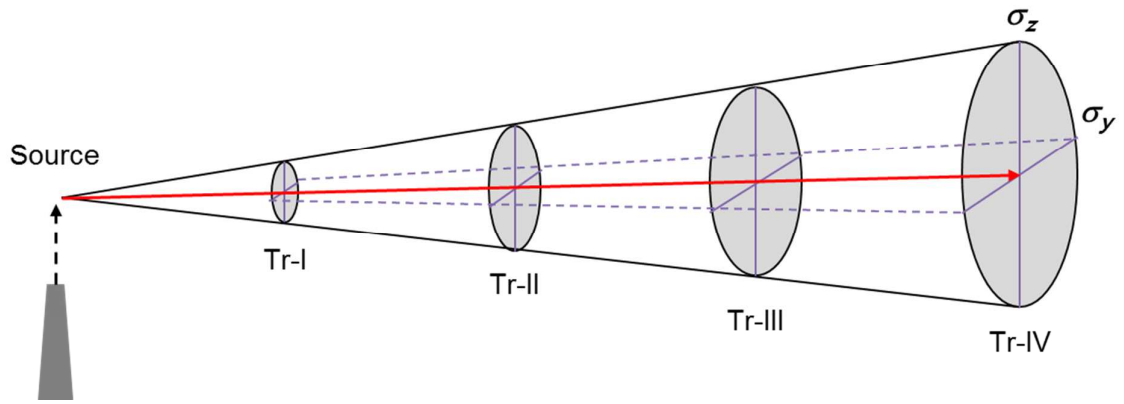

The CO_2 emission rates were calculated by harmonic mean of the CO_2 emission rates estimated from the three sections. Here, each CO_2 emission rate can be expressed as a function of in-plume CO_2 mixing ratios and volumetric flow rates in a section. The emission rates of other primary pollutants such as NO_x, SO_2, and CO were then determined by the aircraft-derived emission ratios, using the CO_2 emission rates estimated from the flight observations for the two power-plant plumes. The aircraft-derived emission ratios for $[NO_x]/[CO_2]$, $[SO_2]/[CO_2]$, and $[CO]/[CO_2]$ were 0.77 ± 0.10, 2.81 ± 0.28, and 5.44 ± 0.27 (ppbv/ppmv), respectively, for Monticello, and 1.19 ± 0.14, 1.50 ± 0.15, and 1.68 ± 0.11 (ppbv/ppmv), respectively, for Welsh.

Determination of plume track and stability classes

In order to determine the plume tracks for Monticello and Welsh plumes, wind speeds and directions were investigated using the horizontal vector components of wind (**u** and **v**) that were obtained from the WRF-simulated outputs. As presented in Fig. 2a and 2b, the wind speeds and directions with the plume-travel (or plume-aging) times range from approximately 6.5 to 9.0 (m s^{-1}) and from 179 to 180° (southerly winds), respectively. It can be noted that the wind directions did not change greatly, however, speeds tended to vary to some extent during the plume-travel time of 150 min. The variable wind speeds were used in the calculation of plume-dispersion coefficients. In addition, in the GIST-RPM simulations, the time-dependent meteorological parameters were selectively taken into account along the interpolated pathways.

The determination of time-dependent changes in the atmospheric stability is necessary to correctly describe the variations in turbulent dispersion. Commonly, there are six atmospheric stability classes: A (very unstable); B (moderately unstable); C (slightly unstable); D (neutral); E (moderately stable); and F (stable). Turner's method for the determination of Pasquill-Gifford stability categories was chosen for the present study, using meteorological parameters (wind velocity at 10 m and net radiation related to the solar altitude) obtained from the WRF model simulation (refer to Figs. 2c and 2d). The atmospheric stability classes estimated along the plume-travel tracks exist between the slightly unstable (C) and neutral (D) conditions (see Fig. 2e). This was briefly confirmed via a comparison between the adiabatic lapse rate and the actual lapse rate obtained from the WRF model simulation.

Table S1. Statistical analysis with aircraft-observed and WRF-modeled meteorological parameters[%]

Statistical parameters	Wind velocity	Temperature	Pressure
RMSE	1.47	0.93	6.33
MNGE	20.09	0.25	0.64
MB	0.30	-0.70	6.01
MNB	9.63	-0.23	0.64

[%] The units of wind velocity, temperature, and pressure for RMSE and MB are meter per second (m/s), kelvin (K), and millibar (mb), respectively, and those for MNGE and MNB are %.

Table S2. Modified reaction-rate coefficients with some reactions, based on Lurmann mechanism

Reactions	Rate constant k (cm^3 $molecule^{-1}$ sec^{-1})	
	Original values[25]	Modified values[26]
$NO + O_3 \rightarrow NO_2 + O_2$	$2.2 \times 10^{-12}e^{-1430/T}$	$3.0 \times 10^{-12}e^{-1500/T}$
$NO + NO_3 \rightarrow 2NO_2$	$8.0 \times 10^{-12}e^{250/T}$	$1.5 \times 10^{-11}e^{170/T}$
$NO_2 + NO_3 \rightarrow NO + NO_2 + O_2$	$2.5 \times 10^{-14}e^{-1230/T}$	$4.5 \times 10^{-14}e^{-1260/T}$
$HNO_3 + OH \rightarrow NO_3 + H_2O$	$9.4 \times 10^{-15}e^{778/T}$	$2.4 \times 10^{-14}e^{460/T}$
$O_3 + OH \rightarrow HO_2 + O_2$	$1.6 \times 10^{-12}e^{-1000/T}$	$1.7 \times 10^{-12}e^{-940/T}$
$NO + HO_2 \rightarrow NO_2 + OH$	$3.7 \times 10^{-12}e^{240/T}$	$3.3 \times 10^{-12}e^{270/T}$
$O_3 + HO_2 \rightarrow OH + 2O_2$	$1.4 \times 10^{-14}e^{-600/T}$	$1.0 \times 10^{-14}e^{-490/T}$
$H_2O_2 + OH \rightarrow HO_2 + H_2O$	$3.1 \times 10^{-12}e^{-187/T}$	1.8×10^{-12}
$NO_2 + H_2O \rightarrow HONO + OH$	4.0×10^{-24}	1.7×10^{-13}
$HNO_4 + OH \rightarrow NO_2 + H_2O + O_2$	4.0×10^{-12}	$1.3 \times 10^{-12}e^{380/T}$
$HCHO + OH \rightarrow HO_2 + CO + H_2O$	1.0×10^{-11}	$5.5 \times 10^{-12}e^{125/T}$
$NO_3 + HCHO \rightarrow HNO_3 + HO_2 + CO$	3.2×10^{-16}	5.1×10^{-16}
$MCO_3 + NO \rightarrow MO_2 + NO_2 + CO_2$	$4.2 \times 10^{-12}e^{180/T}$	$8.1 \times 10^{-12}e^{270/T}$
$CH_4 + OH \rightarrow MO_2 + H_2O$	$2.4 \times 10^{-12}e^{-1710/T}$	$2.5 \times 10^{-12}e^{-1775/T}$
$C_2H_6 + OH \rightarrow ETO_2 + H_2O$	$1.7 \times 10^{-11}e^{-1232/T}$	$7.7 \times 10^{-12}e^{-1020/T}$
$C_3H_8 + OH \rightarrow R_3O_2$	$1.2 \times 10^{-11}e^{-679/T}$	$8.7 \times 10^{-12}e^{-615/T}$

Table S3. Formulas for the later and vertical dispersion parameters, $\sigma_y(x)$ and $\sigma_z(x)$, as a function of the downwind distance, x(m), for rural conditions over land[%]

Pasquill stability class	σ_y (m)	σ_z (m)
For $x < 10$ km		
A	$0.22x(1+0.0001x)^{-1/2}$	$0.20x$
B	$0.16x(1+0.0001x)^{-1/2}$	$0.12x$
C	$0.11x(1+0.0001x)^{-1/2}$	$0.08x\,(1+0.0002x)^{-1/2}$
D	$0.08x(1+0.0001x)^{-1/2}$	$0.06x\,(1+0.0015x)^{-1/2}$
E	$0.06x(1+0.0001x)^{-1/2}$	$0.03x\,(1+0.0003x)^{-1}$
F	$0.04x(1+0.0001x)^{-1/2}$	$0.016x\,(1+0.0003x)^{-1}$
For $x > 10$ km		
A	$0.156x$	$0.20x$
B	$0.113x$	$0.12x$
C	$0.078x$	$0.08x\,(1+0.0002x)^{-1/2}$
D	$0.057x$	$0.06x\,(1+0.0015x)^{-1/2}$
E	$0.042x$	$0.03x\,(1+0.0003x)^{-1}$
F	$0.028x$	$0.016x\,(1+0.0003x)^{-1}$

[%] Briggs (1973)'s dispersion parameters were estimated by combining Pasquill (based on diffusion experiments in Nebraska), BNL (Brookhaven National Lab.), and TVA (Tennessee Valley Authority) curve.

Table S4. Statistical analysis with aircraft-observed and model-calculated concentrations at four plume transects[%]

Species	Monticello						Welsh					
	IOA[a]	R[b]	RMSE[c]	MNGE[d]	MB[e]	MNB[f]	IOA[a]	R[b]	RMSE[c]	MNGE[d]	MB[e]	MNB[f]
NO_x	0.92	0.85	1.63	38.31	-0.19	11.88	0.88	0.80	1.07	78.97	0.21	60.71
SO_2	0.95	0.92	4.58	60.52	-1.50	-5.74	0.81	0.76	2.43	59.05	-0.27	-1.81
O_3	0.77	0.76	3.51	6.69	-1.00	-1.59	0.76	0.77	3.84	7.30	-2.49	-5.47
H_2SO_4	0.77	0.68	2.75	178.28	0.84	135.19	0.77	0.61	2.39	268.55	0.41	240.59

[%] The units for RMSE and MB are ppbv, except for H_2SO_4 in pptv, and those for MNGE and MNB are %.

[a] IOA (Index of agreement)$=1-\frac{\sum_{1}^{N}(C_{i,Model}-C_{i,Obs})^2}{\sum_{1}^{N}(|C_{i,Model}-\overline{C_{i,Obs}}|+|C_{i,Obs}-\overline{C_{i,Obs}}|)^2}$; [b] R (Correlation coefficient)$=\frac{\sum_{1}^{N}(C_{i,Model}-\overline{C_{i,Model}})(C_{i,Obs}-\overline{C_{i,Obs}})}{\sqrt{\sum_{1}^{N}(C_{i,Model}-\overline{C_{i,Model}})^2\sum_{1}^{N}(C_{i,Obs}-\overline{C_{i,Obs}})^2}}$;

[c] RMSE (Root mean square error)$=\sqrt{\frac{1}{N}\sum_{1}^{N}(C_{i,Model}-C_{i,Obs})^2}$; [d] MNGE (Mean normalized gross error)$=\frac{1}{N}\sum_{1}^{N}(\frac{|C_{i,Model}-C_{i,Obs}|}{C_{i,Obs}})\times 100$;

[e] MB (Mean bias)$=\frac{1}{N}\sum_{1}^{N}(C_{i,Model}-C_{i,Obs})$; [f] MNB (Mean normalized bias)$=\frac{1}{N}\sum_{1}^{N}(\frac{C_{i,Model}-C_{i,Obs}}{C_{i,Obs}})\times 100$

Table S5. NO_x chemical lifetimes for several power-plant plumes

NO_x chemical lifetime	Source of plume	Experiment	Estimation method	Ref.
4.4-5.6 hrs	Middle Tennessee power plants	SOS 1995	Aircraft observation	49
2.8-4.2 hrs	Middle Tennessee power plants	SOS 1995	Aircraft observation	50
1.3-3.1 hrs	Eastern Texas power plants	TexAQS 2000	Aircraft observation	52
2.0-6.0 hrs	Southeastern US power plants	NOMADSS	Aircraft observation	55
6.4 hrs	Middle Tennessee power plants	SOS 1995	2-D Lagrangian modeling	51
1.2-2.6 hrs	Eastern Texas power plants	TexAQS II 2006	3-D photochemical modeling	54
1.9-7.5 hrs	China and US power plants	OMI NO_2 data	Satellite observation	56

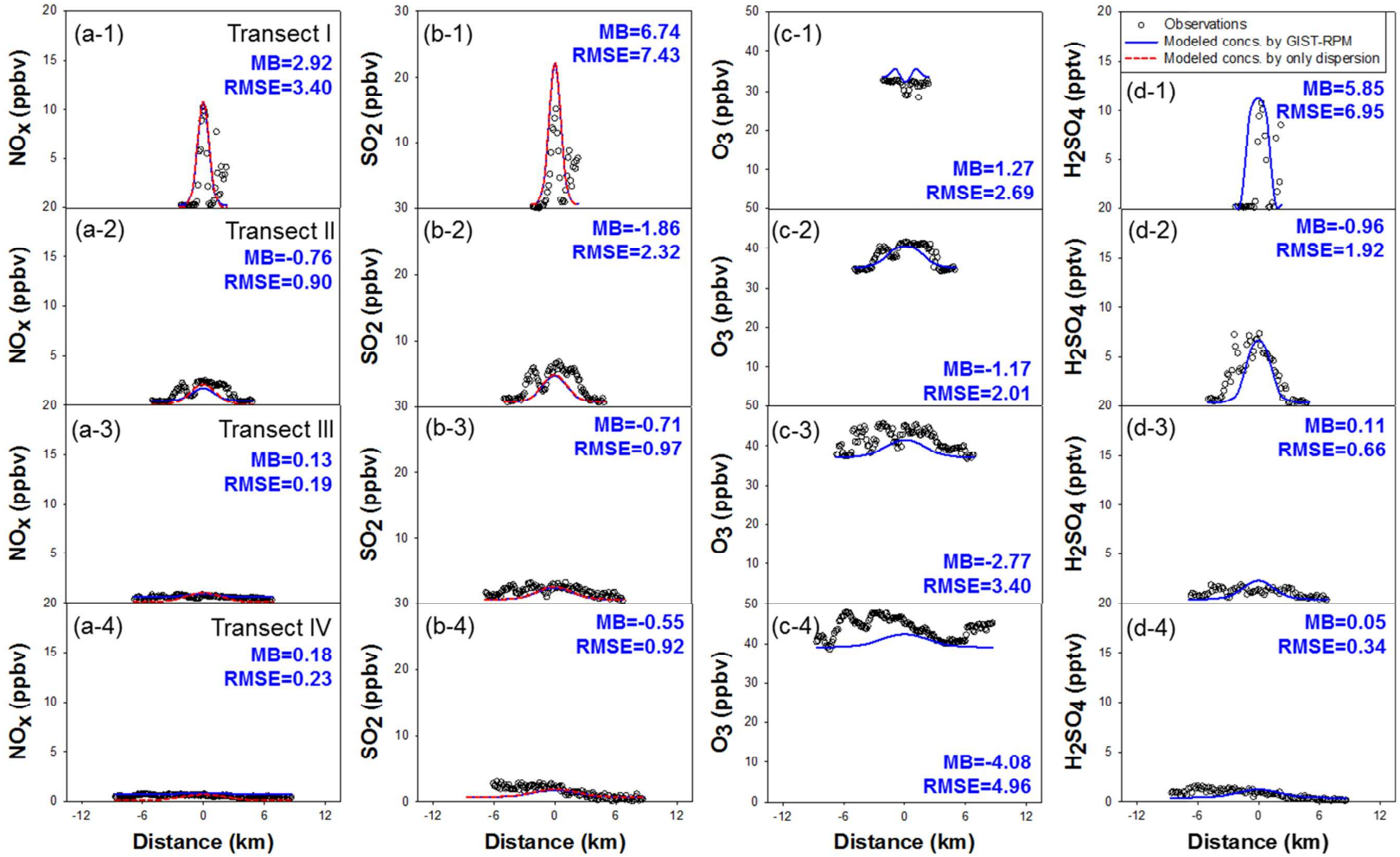

Figure S1. The same as Fig. 3, except for Welsh power-plant plume.

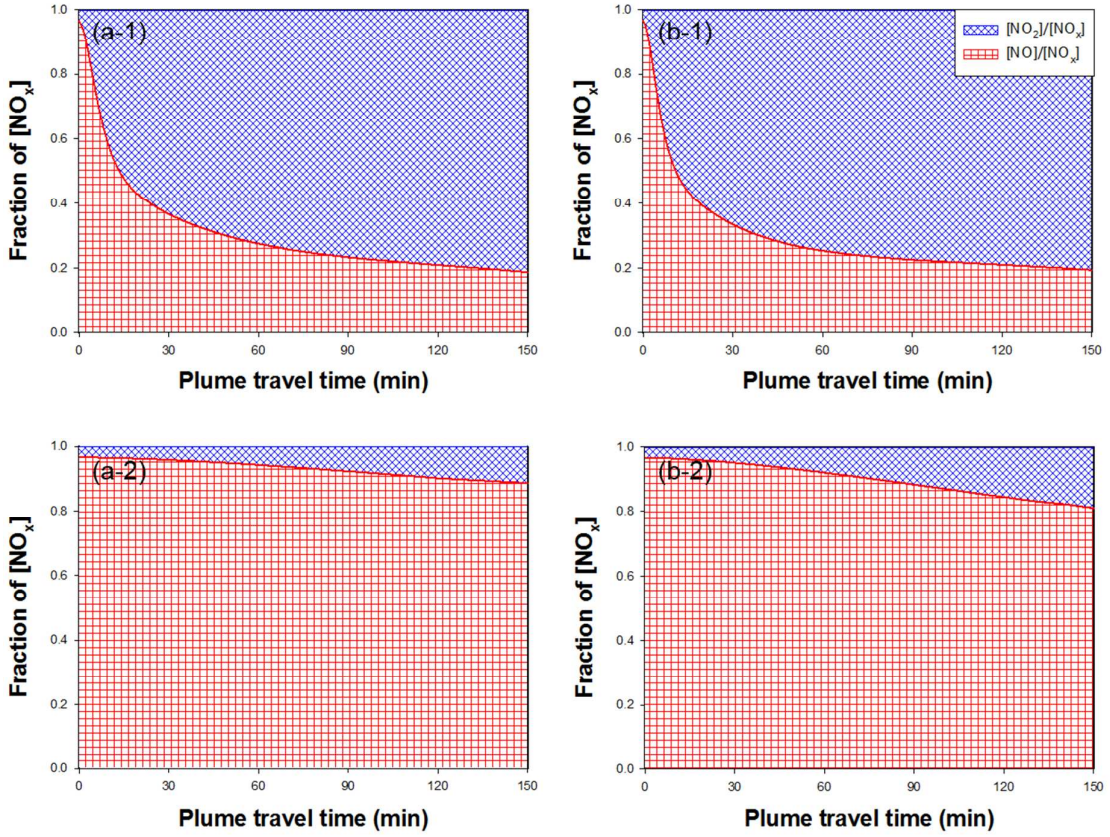

Figure S2. Changes in the NO_x composition along the plume travel times for (a) Monticello and (b) Welsh power plants. The top and bottom panels represent the modeled results with and without the consideration of in-plume photochemistry, respectively.

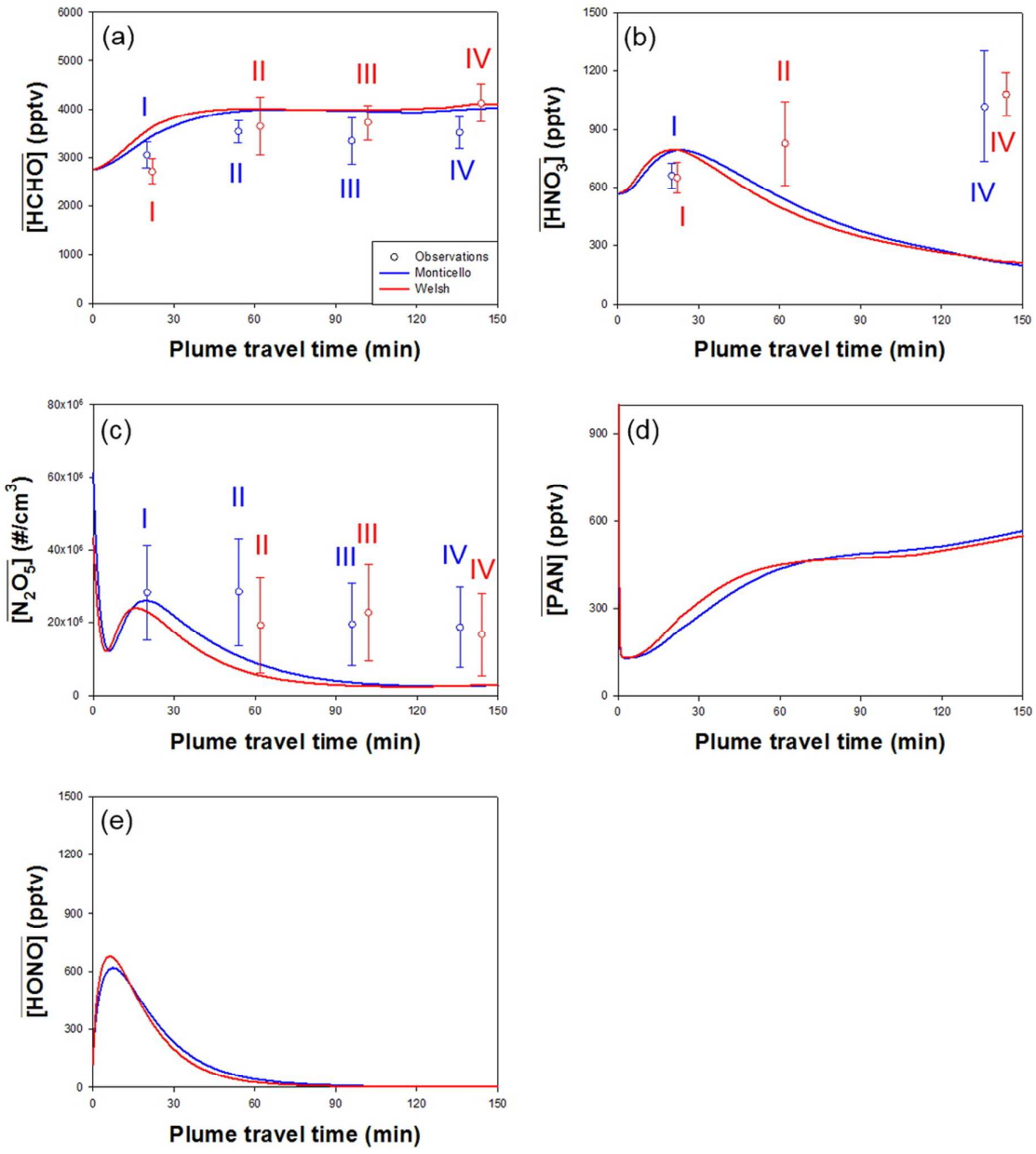

Figure S3. Changes in the concentrations of five secondary species along the plume travel times for Monticello and Welsh power plants: (a) HCHO; (b) HNO_3; (c) N_2O_5; (d) PAN; (e) HONO. The open circles and bars represent the average mixing ratios and standard deviations observed at the four transects (I –IV), respectively. However, it appears that these values should be smaller, given that the observed mixing ratios are larger than the simulated mixing ratios. This should be further investigated with a larger number of data sets. Also, it is shown that HONO mixing ratios build up near the stack. This is certainly related to high NO mixing ratios and concurrent build-ups of OH mixing ratios around the plume-travel time of 10 min.